

Simplified Configuration of a Two-DOF Actively Controlled Bearingless Motor Using Two H-Bridges

Junichi ASAMA*, Kenta SASAKI*, Takaaki OIWA,* and Akira CHIBA**

*Department of Mechanical Engineering, Shizuoka University
3-5-1 Johoku, Naka-ku, Hamamatsu, Shizuoka 432-8561, Japan
E-mail: asama@shizuoka.ac.jp

**Department of Electrical and Electronic Engineering, Tokyo Institute of Technology
2-12-1 Ookayama, Meguro, Tokyo 152-8552, Japan

Abstract

This paper introduces a new structure and topology of a two-degrees-of-freedom (DOF) actively controlled bearingless motor using only two H-bridges (four half-bridges). The proposed two-DOF controlled bearingless motor has two-phase integrated motor windings. The neutral point of each phase winding is connected to the middle point of the inverter's dc power voltage. This bearingless motor, thus, offers common dq -axis current vector control for permanent magnet motor drive as well as radial two-DOF active positioning control of the rotor. In this paper, the suspension force and torque of the 2-pole/8-slot model are theoretically derived from the stored magnetic energy. The magnetic energy is calculated from the inductance matrix where each inductance component is derived with the air-gap magnetic flux distribution. The theoretically calculated results show how the suspension force and torque are regulated with the control currents. To verify the theoretical calculation, two-dimensional FEM analysis is performed. The FEM calculation demonstrates that the proposed bearingless motor topology with 2-pole/8-slot structure using only two H-bridges generates constant suspension force and torque.

Keywords : Bearingless motor, Magnetic bearing, Integrated winding, Two-DOF active positioning control

1. Introduction

Various types of bearingless motors with two-degrees-of-freedom (DOF) active positioning control in the radial direction of the rotor have been previously proposed. Some bearingless motors use two kinds of windings for motor drive and magnetic suspension, which are separately wound in the single stator. For instance, a bearingless permanent magnet (PM) motor with a p -pole rotor has additional $(p+2)$ - or $(p-2)$ -pole field winding for surface-mounted PM rotor suspension (Ooshima et al., 1996, Schöb and Barletta, 1996) or for 2-pole field winding for homo-polar and consequent-pole PM rotor suspension (Ichikawa, et al., 2001, Asama, et al., 2013). The slot space of these bearingless PM motors is occupied by both motor and suspension windings.

Other bearingless motors employ only motor winding which can generate not only torque but also suspension force. Hence, such a motor winding that integrates magnetic suspension function is called an integrated winding in this paper. Based on the three-phase motor structure, inverters (Chiba, et al., 2011, Ooshima, et al., 2011, Oishi, et al., 2013), current amplifiers (Salazar and Stephan, 1993, Khoo, et al., 2002), or four power transistors (Miyashita, et al., 2011) are additionally used to superimpose the suspension current into the integrated motor windings. Bearingless poly-phase PM motors, which use several half-bridges to regulate the currents flowing in the poly-phase integrated motor winding, have been proposed (Amrhein and Silber, 1998, Gruber, et al., 2009, Bartholet, et al., 2009).

In particular, the bearingless four-pole PM motor, introduced by Bartholet, et al. (2009), has four coils (four-phase winding) and uses only four half-bridges to control three independent currents. A two-DOF controlled bearingless 6-pole PM motor, developed by Oi, et al. (2015), has two separated windings, but is driven by only one three-phase inverter (three half-bridges). These bearingless PM motors have the reduced number of power transistors, which can contribute to cost reduction. These machines, however, offer single-phase motor drive, and thus, common dq -axis

current vector control for highly efficient PM motor drive cannot be applied. This paper concerns a new topology for a bearingless PM motor with two-DOF active positioning. The proposed bearingless motor topology has only integrated motor winding configuration, uses only two H-bridges (four half-bridges), and offers the dq -axis current vector control for PM motor drive.

2. Proposed Bearingless Motor Topology

Fig. 1 shows a structure of the 2-pole/8-slot bearingless PM motor that has two-phase integrated motor winding for both motor drive and magnetic suspension. Fig. 2 shows the inverter topology using two H-bridges. The bearingless motor has two phases using concentrated coils, denoted by a - and b -phase. One phase consists of 4 coils which are connected in series. The neutral point of one phase is connected to the middle point of the inverter's dc voltage. Two current components for rotation and magnetic suspension are superimposed into the two-phase winding. The four-phase topology using four half-bridges, where the four coils are connected in star, can also be used, when the neutral point of the star-connected winding is shorted to the middle point of the inverter's dc voltage. It is important for the proposed topology to regulate four independent currents, i_{a1} , i_{a2} , i_{b1} , and i_{b2} , with the reduced number of eight power transistors.

When the power transistors, s_1 and s_4 , are turned on, for instance, the a -phase motor current, i_{ma} , flows as shown with red line in Fig. 2, which produces 2-pole magnetic field. In a similar manner, the b -phase motor current, i_{mb} , which is independent on i_{ma} , also produces 2-pole magnetic field. The a -phase suspension current, i_{sa} , flows when the power transistors, s_1 and s_3 , are turned on, as shown in blue lines in Fig. 2. In this case, the teeth of a_1 and a_3 are excited to S -pole whereas the teeth of a_2 and a_4 are excited to N -pole, resulting in 4-pole field generation. The b -phase suspension current, i_{sb} , also generates 4-pole field. The suspension force is generated in the radial direction by superimposition of the 4-pole fields with the rotor's bias 2-pole field. This topology with integrated motor winding offers both two-DOF active positioning and dq -axis current-based motor drive control using only two H-bridges.

3. Theoretical Calculation for Suspension Force and Torque

3.1 Permeance Variation

This section considers theoretical calculation for suspension force and torque of the proposed model. The air-gap permeance variation caused by the slight displacement of the rotor in the radial direction is derived. The radial displacement, x and y , is much smaller than the air-gap and the rotor radius. It is assumed that the rotor and stator surfaces are cylindrical and thus the stator slot harmonics are neglected. The air-gap permeance distribution, P , at an angular position of the stator, ϕ_s , can be geometrically derived (Chiba, et al., 2005), and written as

$$P(\phi_s) = \frac{\mu_0 R l}{g_0} \left(1 + \frac{x}{g_0} \cos \phi_s + \frac{y}{g_0} \sin \phi_s \right) \quad (1)$$

where μ_0 is space permeability, R is the rotor radius, l is the axial length, g_0 is the nominal air-gap.

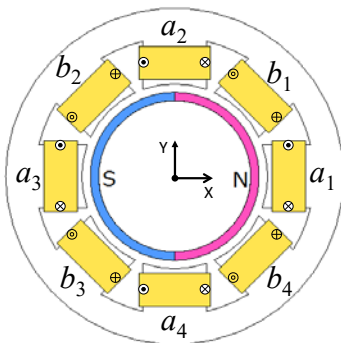


Fig. 1 2-pole/8-slot two-phase bearingless PM motor.

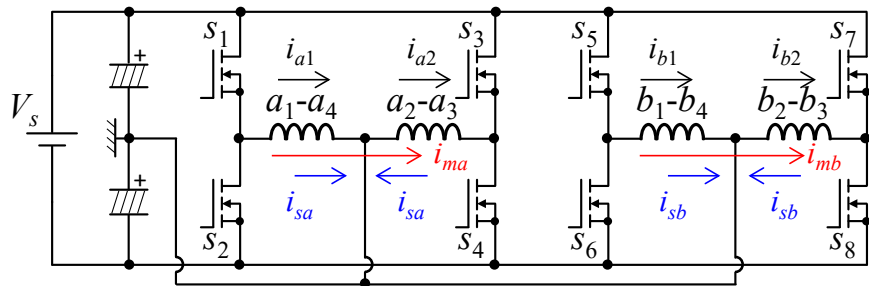


Fig. 2 Proposed inverter topology for two-phase bearingless PM motor using integrated motor winding and two H-bridges (four half-bridges).

3.2 MMF Distribution

The magneto-motive force (MMF) distributions for a_1 and a_4 coils with unity current, A_{a1} and A_{a4} , are approximated by

$$A_{a1}(\phi_s) = N\{a_0 + a_1 \cos \phi_s + a_2 \cos 2\phi_s\} \quad (2)$$

$$A_{a4}(\phi_s) = -N\left\{a_0 + a_1 \cos\left(\phi_s - \frac{3\pi}{2}\right) + a_2 \cos 2\left(\phi_s - \frac{3\pi}{2}\right)\right\} \quad (3)$$

where N is the number of coil turns and a_0 , a_1 , and a_2 are the amplitudes of dc, 1st and 2nd harmonic components, respectively. The a_1 and a_4 coils are connected in series. The sum of these MMFs, A_{a14} , as shown in Fig. 3, can be written as

$$A_{a14}(\phi_s) = A_{a1} + A_{a4} = N\{a_1(\cos \phi_s + \sin \phi_s) + 2a_2 \cos 2\phi_s\} \quad (4)$$

In a similar manner, the MMF distributions caused by other winding sets, A_{a23} , A_{b14} , and A_{b23} can be derived.

The permanent magnet of the rotor can be replaced with equivalent winding. The magnet MMF distribution with unity current, A_p , is approximated by sinusoidal, and hence written as

$$A_p(\phi_s) = N_p \cos(\phi_s - \theta) \quad (5)$$

where N_p is the equivalent number of turns and θ is the rotational angle of the rotor from the X-axis. When the rotor's N-pole aligns with the center of the a_1 tooth, the rotational angle is $\theta = 0^\circ$.

3.3 Flux Distribution

Fig. 4 shows the magnetic circuit when only a_1 and a_4 coils are excited. The voltage, V_{a14} , represents the magnetic potential of the rotor. Hence, the magnetic flux, ψ_{a14} , in one branch is written as

$$\psi_{a14} = P(A_{a14} + V_{a14}) \quad (6)$$

According to Gauss's law, an integral of the magnetic flux around the rotor surface must be zero. Hence, the following equation is obtained

$$V_{a14} = -\frac{\int_0^{2\pi} (PA_{a14})d\phi_s}{\int_0^{2\pi} Pd\phi_s} = -\frac{Na_1}{2g_0}(x+y) \quad (7)$$

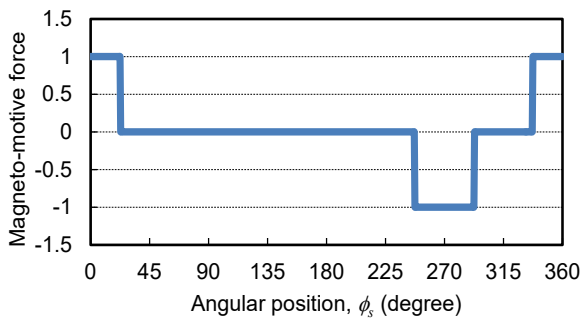


Fig. 3 Magneto-motive force distribution for a_1 and a_4 coils with unity current, A_{a14} .

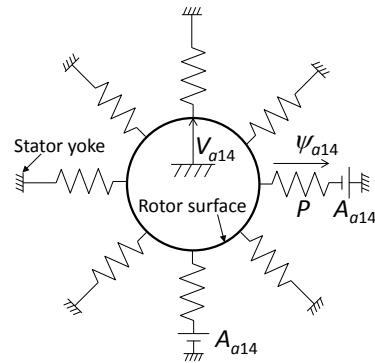


Fig. 4 Magnetic circuit with excitation of a_1 and a_4 coils.

The magnetic flux distribution produced by a_1 and a_4 coils with unity current excitation is written as

$$\psi_{a14}(\phi_s) = \frac{\mu_0 R I N}{2g_0^3} (g_0 + x \cos \phi_s + y \sin \phi_s) \{a_1(2g_0 \cos \phi_s + 2g_0 \sin \phi_s - x - y) + 4a_2 g_0 \cos 2\phi_s\} \quad (8)$$

In a similar manner, the flux distributions, ψ_{a23} , ψ_{b14} , and ψ_{b23} can be derived.

We concern the magnetic circuit when the equivalent winding of the permanent magnet is excited. The voltage, V_p , represents the magnetic potential of the rotor. The magnetic flux caused by the permanent magnet, ψ_p , is written as

$$\psi_p = P \left(\frac{1}{2} A_p + V_p \right) \quad (9)$$

An integral of the magnetic flux around the rotor surface is zero, thus, V_p results in

$$V_p = -\frac{\frac{1}{2} \int_0^{2\pi} (P A_p) d\phi_s}{\int_0^{2\pi} P d\phi_s} = -\frac{N_p}{4g_0} (x \cos \theta + y \sin \theta) \quad (10)$$

The magnetic flux distribution caused by the permanent magnet unity current excitation is written as

$$\psi_p(\phi_s) = \frac{\mu_0 R I N_p}{4g_0^3} (g_0 + x \cos \phi_s + y \sin \phi_s) \{x \cos \theta + y \sin \theta - 2g_0 \cos(\phi_s - \theta)\} \quad (11)$$

3.4 Inductance and Magnetic Energy

The inductance can be derived by integral of the product of magnetic flux and winding distribution, where the winding distribution is equivalent to the MMF distribution per unity current. The self-inductance of the a_1 and a_4 coils, L_{a14} , is expressed as

$$L_{a14} = \int_0^{2\pi} (\psi_{a14} A_{a14}) d\phi_s \approx \frac{2\pi\mu_0 R I N^2}{g_0^2} \{g_0(2a_2^2 + a_1^2) + a_1 a_2(x - y)\} \quad (12)$$

The products of small displacements are ignored in the above equation. The mutual-inductances between the a_1 - a_4 and a_2 - a_3 windings, M_{a1a2} , a_1 - a_4 and b_1 - b_4 windings, M_{a1b1} , and a_1 - a_4 and equivalent magnet windings, M_{a1p} are expressed as

$$M_{a1a2} = \int_0^{2\pi} (\psi_{a14} A_{a23}) d\phi_s \approx \frac{2\pi\mu_0 R I N^2}{g_0} (a_1^2 - 2a_2^2) \quad (13)$$

$$M_{a1b1} = \int_0^{2\pi} (\psi_{a14} A_{b14}) d\phi_s \approx \frac{\pi\mu_0 R I N^2 a_1}{g_0^2} \{\sqrt{2}a_1 g_0 + a_2(x + y - \sqrt{2}y)\} \quad (14)$$

$$M_{a1p} = \frac{1}{2} \int_0^{2\pi} (\psi_{a14} A_p) d\phi_s \approx \frac{\pi\mu_0 R I N_p}{2g_0^2} \{(a_1 g_0 + a_2 x) \cos \theta + (a_1 g_0 - a_2 y) \sin \theta\} \quad (15)$$

The self-inductance of the permanent magnet coil, L_p , and the mutual-inductance between a_1 - a_4 and equivalent magnet windings, M_{pa1} , can be derived as

$$L_p = \frac{1}{2} \int_0^{2\pi} (\psi_p A_p) d\phi_s \approx \frac{\pi\mu_0 R I N_p^2}{4g_0} \quad (16)$$

$$M_{pa1} = \int_0^{2\pi} (\psi_p A_{a14}) d\phi_s \approx \frac{\pi\mu_0 R I N N_p}{2g_0^2} \{(a_1 g_0 + a_2 x) \cos \theta + (a_1 g_0 - a_2 y) \sin \theta\} = M_{a1p} \quad (17)$$

In a similar manner, other self- and mutual-inductances can be calculated, and thus, a 5×5 inductance matrix, \mathbf{L} , is obtained. Then, the stored magnetic energy, W_m , is given by

$$W_m = \frac{1}{2} \mathbf{i}^T \mathbf{L} \mathbf{i} \quad (18)$$

where,

$$\mathbf{i} = \begin{bmatrix} I_p \\ i_{a1} \\ i_{a2} \\ i_{b1} \\ i_{b2} \end{bmatrix} = \begin{bmatrix} I_p \\ i_{ma} + i_{sa} \\ i_{ma} - i_{sa} \\ i_{mb} + i_{sb} \\ i_{mb} - i_{sb} \end{bmatrix} \quad (19)$$

I_p is the dc bias current of the equivalent magnet winding, and i_{a1} , i_{a2} , i_{b1} , and i_{b2} are the currents of the a_1 - a_4 , a_2 - a_3 , b_1 - b_4 , and b_2 - b_3 coils, respectively.

3.5 Suspension Force and Torque

The suspension force can be derived from the partial derivative of the stored magnetic energy, W_m , with respect to the rotor displacement

$$F_x = \frac{\partial W_m}{\partial x} = \frac{\pi\mu_0 R I N a_2}{g_0^2} \left[N_p I_p (i_{sa} \cos \theta + i_{sb} \sin \theta) + 4N a_1 \{ i_{ma} (i_{sa} + i_{ba}) + \sqrt{2} i_{mb} i_{sb} \} \right] \quad (20)$$

The torque can also be derived from the partial derivative of the stored magnetic energy, W_m , with respect to the rotational angle, θ . When the rotor is located at the center of the stator bore, the torque, T , is written as

$$T = \frac{\partial W_m}{\partial \theta} = \frac{\pi\mu_0 R I N N_p I_p a_1}{g_0} \{ i_{ma} (\cos \theta - \sin \theta) + \sqrt{2} i_{mb} \cos \theta \} \quad (21)$$

The equations (20) and (21) show how the suspension force and torque are regulated with the control currents.

4. FEM Calculation

To verify the theoretical calculation, two-dimensional FEM calculation is performed with a commercially available software (JMAG, JSOL Corp., Japan). The analysis model is an inner rotor type of 2-pole/8-slot bearingless PM motor. The rotor outer diameter is 40 mm, and the radial magnet thickness is 4 mm. The magnet material is NdFeB (N35 grade). The nominal air-gap between the magnet surface and teeth inner surface is 2 mm. The tooth width and radial thickness of the stator back yoke are 15 mm and 17 mm, respectively. The outer stator diameter is 120 mm. The axial stack length is set to be 20 mm. The amplitude of the applied sinusoidal current is 84 A·turns.

Fig. 5 shows the calculated suspension force in the X-axis, F_x , when $i_{ma} = i_{mb} = 0$ A. The average and peak-to-peak values are 9.5 N and 0.06 N, respectively. The constant force is available at all rotational angles. The interference angle, which is defined as an angle between the X-axis suspension force and undesirable Y-axis force with X-axis current, is smaller than 0.4° (the graph is not shown). Fig. 6 shows the calculated torque when $x = y = 0$. The average is 31 mNm whereas the torque ripple with peak-to-peak value of 4 mNm is observed. The peak-to-peak value of the cogging torque is approximately 1 mNm, hence, this torque ripple may be caused by the MMF harmonic components.

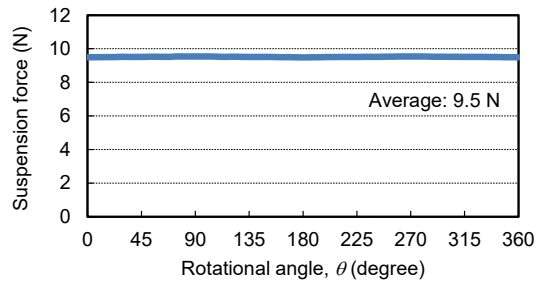


Fig. 5 Calculated suspension force in the X-axis, F_x , without motor current.

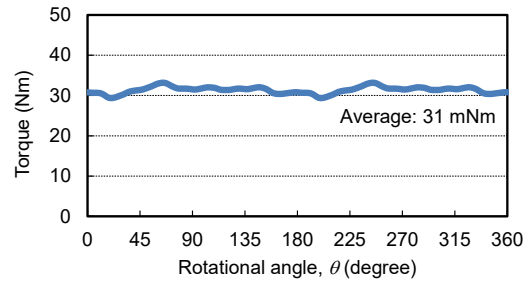


Fig. 6 Calculated torque, T , without radial displacement.

5. Conclusion

We propose a new structure and topology of a two-DOF actively controlled bearingless motor that uses only two H-bridges (four half-bridges). This bearingless motor has 2-pole/8-slot rotor structure and has two-phase integrated motor winding. The suspension force and torque are theoretically derived. The FEM calculation demonstrates that the proposed structure can generate acceptable suspension force and torque. In future works, we will consider the influence of the motor current on the radial force, and built a test machine to verify the proposed method experimentally.

References

- Amrhein, W. and Silber, S., "Bearingless Single-Phase Motor with Concentrated Full Pitch Windings in Interior Rotor Design", Proceedings of the 6th International Symposium on Magnetic Bearings, pp. 486-496, 1998.
- Asama, J., Kanehara, D., Oiwa, T., and Chiba, A., "Suspension Performance of a Two-Axis Actively Regulated Consequent-Pole Bearingless Motor", IEEE Transactions on Energy Conversion, Vol. 28, No. 4, pp. 894-901, 2013.
- Bartholet, M. T., Nussbaumer, T., Silber, S., and Kolar, J. W., "Comparative Evaluation of Polyphase Bearingless Slice Motors for Fluid-Handling Applications," IEEE Transactions on Industry Applications, Vol. 45, No. 5, pp. 1821-1830, September/October 2009.
- Chiba, A., Fukao, T., Ichikawa, O., Masahide, O., Takemoto, M., and Dorrell, D. G., "Magnetic Bearings and Bearingless Drives", Elsevier, 2005.
- Chiba, A., Sotome, K., Iiyama, Y., and Rahman, M.A., "A Novel Middle-Point-Current-Injection-Type Bearingless PM Synchronous Motor for Vibration Suppression," IEEE Transactions on Industry Applications, Vol. 47, No. 4, pp. 1700-1706, July/August 2011.
- Gruber, W., Amrhein, W., and Haslmayr, M., "Bearingless segment motor with five stator elements—Design and optimization," IEEE Transactions on Industry Applications, Vol. 45, No. 4, pp. 1301-1308, July/August 2009.
- Ichikawa, O., Chiba, A., and Fukao, T., "Inherently decoupled magnetic suspension in homopolar-type bearingless motors", IEEE Transactions on Industry Applications, Vol. 37, No. 6, pp. 1668-1674, Nov./Dec. 2001.
- Khoo, S. W. K., Fittro, R. L., and Garvey, S. D., "AC Polyphase Self-Bearing Motors with a Bridge Configured Winding", Proceedings of the International Symposium on Magnetic Bearings, Mito, Japan, August 26-28, 2002.
- Miyashita, K., Ooshima, M., and Uddin, M. N., "Design of a Time-Divided Torque and Suspension Force Control Type Bearingless Motor", Proceedings of the 2011 IEEE Power and Energy Society General Meeting, San Diego, CA, USA, 24-29 July, 2011
- Oi, T., Asama, J., Oiwa, T., and Chiba, A., "A Two-DOF Actively Positioned Bearingless Motor Using One Three-Phase Inverter," Proceedings of the IEEJ Industry Applications Society Conference, Y-123, 2015 (in Japanese).
- Oishi, R., Horima, S., Sugimoto, H., and Chiba, A., "A Novel Parallel Motor Winding Structure for Bearingless Motors," IEEE Transactions on Magnetics, Vol. 49, No. 5, pp. 2287-2290, May 2013.
- Ooshima, M., Chiba, A., Fukao, T., and Rahman, M. A., "Design and Analysis of Permanent Magnet-Type Bearingless Motors," IEEE Transaction on Industrial Electronics, Vol. 43, No. 2, pp. 292-299, April 1996.
- Schöb, R. and Barletta, N., "Principle and Application of a Bearingless Slice Motor", Proceedings of the 5th International Symposium on Magnetic Bearings, pp. 313-318, Kanazawa, Japan, August, 1996.